Fluctuations and Anharmonicity in Lead Iodide Perovskites from Molecular Dynamics Supercell Simulationss

Marcelo Andrés Carignano, S. Assa Aravindh, Iman S Roqan, Jacky Even, Claudine Katan

Journal of Physical Chemistry C, American Chemical Society, 2017, 121 (38), pp.20729-20738. ⟨10.1021/acs.jpcc.7b08220⟩

Critical Fluctuations and Anharmonicity in Lead Iodide Perovskites from Molecular Dynamics Supercell Simulations

Marcelo A. Carignano,*,† S. Assa Aravindh,‡ Iman S. Roqan,‡ Jacky Even,¶ and Claudine Katan*,§

†*Qatar Environment and Energy Research Institute, Hamad bin Khalifa University, P.O. Box 5825, Doha, Qatar*

‡*Physical Sciences and Engineering, King Abdullah University of Science and Technology (KAUST), Thuwal, Saudi Arabia*

¶*FOTON, UMR6082, CNRS, INSA de Rennes, Avenue des Buttes de Coësmes, 35708 Rennes, France*

§*Institut des Sciences Chimiques de Rennes, UMR6226, CNRS, Université de Rennes 1, Ecole Nationale Suprieure de Chimie de Rennes, INSA de Rennes, 35042 Rennes Cedex, France*

E-mail: mcarignano@hbku.edu.qa; claudine.katan@univ-rennes1.fr

Journal of Physical Chemistry C, American Chemical Society, 2017, 121 (38), pp.20729-20738. ⟨10.1021/acs.jpcc.7b08220⟩

Abstract

We present a systematic study based on first principles molecular dynamics simulations of lead iodide perovskites with three different cations, including methylammonium (MA), formamidinium (FA) and cesium. Using the high temperature perovskite structure as a reference, we investigate the instabilities that develop as the material is cooled down to 370 K. All three perovskites display anharmonicity in the motion of the iodine atoms, with the stronger effect observed for the $MAPbI_3$ and $CsPbI_3$. At high temperature, this behavior can be traced back to the reduced effective size of the Cs^+ and MA^+ cations. $MAPbI_3$ undergoes a spontaneous phase transition within our simulation model driven by the dipolar interaction between neighboring MA cations as the temperature is decreased from 450 K. The reverse transformation from tetragonal to cubic is also monitored through the large distribution of the octahedral tilting angles accompanied by an increase in the anharmonicity of the iodine atoms motion. Both MA and FA hybrid perovskites show a strong coupling between the molecular orientations and the local lattice deformations, suggesting mixed order-disorder/displacive characters of the high temperature phase transitions.

1 Introduction

Hybrid perovskites are at the center of an intense research activity due to their impressive achievements for optoelectronic applications, mainly including solar energy harvesting[1–5] but also photoluminescent devices[6–11] and lasing.[12–14] In this scenario of potential commercial applications, the main driver for research is the development of efficient and durable devices able to challenge the current standard. From the theoretical point of view the subject has attracted considerable attention, as the system represent a challenge and an opportunity to test first principles modeling tools.[15] An important issue affecting this class of material is the anharmonicity in the lattice vibrations that is present in hybrid[16] as well as in purely inorganic perovskites.[17–19] The theoretical basis underlying the importance of anharmonicity

on phase transitions was pioneered by T. Matsubara[20,21] on different crystal structures. For hybrid perovskites, this behavior has further implications in the carrier transport and therefore needs to be addressed in order to understand the underlying physics of perovskite based devices.[22]

This paper focuses on the ground state physico-chemical properties of halide perovskites. We consider two hybrid compounds: methylammonium (MA) lead iodide ($CH_3NH_3PbI_3$ or $MAPbI_3$)[23] and formamidinium (FA) lead iodide ($HC(NH_2)_2PbI_3$ or $FAPbI_3$).[24,25] For comparison purposes, the full inorganic $CsPbI_3$ perovskite is also studied. The two hybrid systems were previously studied by us using first principles molecular dynamics simulations.[26–28] Here we present further simulations that provide a comprehensive analysis at thermodynamic conditions corresponding to their cubic phases and tetragonal phase for $MAPbI_3$, with particular emphasis on critical fluctuations and anharmonicity. The contrast between the three systems helps to shed light into their atomistic organization and dynamics. Moreover, the subtle differences between the two hybrid compounds represent a test bench that allows to evaluate the relevance and predicting power of *state-of-the-art* first principles molecular dynamics simulations.

The three targeted systems have the same inorganic framework and the only difference in the composition is the monovalent cation. For the $MAPbI_3$ case, the carbon and nitrogen atoms of the MA molecule lead to an appreciable net dipole moment of *ca.* 2 D. Conversely, the planar FA molecule, slightly larger than MA, has an almost vanishing dipole moment. Therefore, it is possible to assess the importance of the dipole–dipole correlations across different structural units by making the proper comparison between these two systems. Yet, this is not a straightforward task because of other structural instabilities affecting the systems and that are also present in the purely atomic $CsPbI_3$ perovskite. Another important issue is the coupling between the orientation of the organic cation and the local deformation of the inorganic lattice. This dynamical coupling is driven by the symmetry and size of the cation, which does not conform with the site symmetry at the center of the cubic cell experimentally

reported for the high temperature phase.[23,24,29] In addition, the large anisotropic motion of the halide atoms has also been clearly revealed by crystallographic characterizations, in both inorganic and hybrid compounds.[29–31] As the overall average structure is cubic in the high temperature phase, the cation/lattice coupling is expected to be dynamic and local.

On approaching continuous phase transitions, this coupling may occur over long distances associating phonons and collective molecular pseudospins,[27] as shown recently by molecular dynamics simulations evidencing antiferroelectric molecular fluctuations[32] and measurements of low frequency acoustic phonons.[33] This leads us to introduce characteristics time and length that determine the average lifetime (t_{lc}) and size (λ_{lc}) of local domains having a specific deformation pattern. We should mention here that the molecular character of the cation plays a crucial role in stabilizing the perovskite structure by providing a significative entropic contribution to the free energy. Indeed, the purely atomic $CsPbI_3$ only exhibits the cubic perovskite structure at very high temperature. Therefore, the accounting for the *plastic crystal* character of the hybrid perovskites is essential in order to achieve a comprehensive understanding of these peculiar semiconductors, including the exact sequence of phase transitions,[27,34] related to various structural instabilities at the Γ, M and R points of the perovskite Brillouin zone.[27] The comparison with $CsPbI_3$, also studied here within the same theoretical approach, allows to gauge the importance of the sole lattice anhamonicity,[19] as observed experimentally in the past for $CsPbCl_3$.[35]

A second important difficulty is the result of the high computational cost of the NPT MD simulations. With respect to the system size, we limit ourselves to 64 unit cells that span over 25 Å, approximately. For the dynamic integration process, we extend the trajectories up to $\sim$50 ps. Apart from two recent works where an NVT ensemble was used,[32,36] these two limits are the largest among the similar works reported in the literature and are sufficiently small as to allow for a systematic study. Namely, with these constraints we can afford several runs and this is essential to gain a significant level of confidence in the overall outcome. Noteworthy, the analysis should be done keeping in mind that if $\lambda_{lc} \gtrsim 25$ Å, the simulation results are

affected by the periodic boundary conditions. Similarly, if a process has a characteristic time $t_{lc} \gtrsim 25$ ps, information related to that process may be completely absent from the trajectories.

The structural evolution of $MAPbI_3$ with varying temperature has been known for a long time and its cubic α-phase ($Pm\bar{3}m$) is stable above 327 K, below which lies the tetragonal β-phase (I4/mcm). Depending on the growth conditions, $FAPbI_3$ can crystallized either in a black perovskite phase or in a yellow non perovskite phase. High resolution neutron diffraction experiments[37] have recently confirmed that an α phase, similar to that of $MAPbI_3$, can be stabilized at 300K. The full inorganic $CsPbI_3$ has a similar α-phase and transforms to a yellow non-perovskite structure within a temperature range of 563 to 602 K.[38] Having no molecular cation, $CsPbI_3$ constitutes a simple reference system.

2 Methods

This study relies on first principles molecular dynamics simulations as implemented in CP2K.[39–41] The electron density is represented by the GPW method that combines Gaussian basis sets with auxiliary plane waves defined by an energy cutoff of 300 Ry. All the settings relative to the density functional theory approach are the same as in our previous works on similar systems: PBE functional, Grimme D3 correction scheme for the dispersion interactions,[42,43] DZVP-MOLOPT basis sets[44] and norm-conservative GTH pseudopotentials.[45,46] All the atoms are explicitly represented with their real masses. The molecular dynamics was done under NPT–F conditions, which allow volume fluctuations by changing the supercell edges and angles. The temperature was controlled by a Nose-Hoover thermostat with three chains and the pressure was controlled by the Martyna's barostat.[47] The time constant for both, the thermostat and barostat, was set at 50 fs.

All simulations for the α-phase are based on a $4 \times 4 \times 4$ supercell obtained by replicating the cubic unit cell four times in each Cartesian direction. Therefore, the supercell contains

768 atoms and 64 stoichiometric units for the MA and FA hybrid perovskites. The Cs based perovskite model system has 320 atoms. The procedure to perform the MD simulations starts by heating the initial frozen configuration up to 450 K, followed by a run covering over 50 ps in all cases. For the $MAPbI_3$ case, the initial 45 ps of the trajectory were lost in hardware failure, and the results shown are a continuation with a redefinition of the time axis to start from well equilibrated thermal conditions. A second series of simulations was then performed for each system with the thermostat set at 370 K, starting with the equilibrated configuration at 450 K and its corresponding velocities.

A third set of simulations was carried out for the $MAPbI_3$ perovskite. In this case, the initial structure was prepared using the atomic coordinates of the tetragonal phase as provided in.[48] The supercell was rotated 45° about the z axis in order to match the standard orientation of the cubic phase that we use as overall reference. The system was slowly heated up to 300 K and then a long trajectory was produced. Successive simulations were then performed at 320 K, 340 K, 360 K, 375 K, 385 K and 400 K. The final configuration (or a sufficiently equilibrated one) at a given temperature was used to start the trajectory at the next higher temperature. The highest temperatures (385 K and 400 K) were started from the same structure extracted at 375 K.

3 Results

For the sake of clarity we organized this section in four parts. First, we consider the three systems at high temperature, which we use as the reference states since they all behave in a similar way. Next we analyze in the second part the findings related to $FAPbI_3$ at 370 K that departs from its reference state but still remains cubic. The third part refers to $MAPbI_3$ at 370 K that reveals increasing complexity as compared to $FAPbI_3$ and requires a more elaborated analysis. Finally, in the fourth part, the behavior of $MAPbI_3$ upon heating is investigated, starting from a tetragonal structure. Some results from the $CsPbI_3$ perovskites

are included wherever appropriate.

3.1 High temperature reference states and anharmonicity in $MAPbI_3$ and $CsPbI_3$

We start by considering the time evolution of the lattice parameters for both $MAPbI_3$ and $FAPbI_3$ compounds (Figure 1a) at 450 K. Let us recall that this high temperature was purposely selected in order to study the systems comfortably in the cubic phase and indeed they maintain a cubic structure after 50 ps of MD trajectory. For $MAPbI_3$, it is clear that there are some crossings between the three lines, i.e. lengths of the edges, while for $FAPbI_3$ the three dimensions appear on top of each other. The magnitude of the structural fluctuations are larger in $MAPbI_3$ than in $FAPbI_3$. Moreover, the spontaneous fluctuations of the symmetrized strains can be analyzed according to.[49] Volumetric, orthorhombic and tetragonal strain read $e_a = e_1+e_2+e_3$, $e_{oz} = e_1-e_2$ and $e_{tz} = 1/\sqrt{3}(2e_3-e_1-e_2)$, respectively. $MAPbI_3$ has a stronger tendency to undergo large transient orthorhombic distortions ($\delta e_{oz} = 0.011$), as compared to $FAPbI_3$ ($\delta e_{oz} = 0.008$). The lattice parameter resulting from the average of the trajectories are $a = 6.40 \pm 0.12$ Å and 6.50 ± 0.10 Å for $MAPbI_3$ and $FAPbI_3$, respectively. The effective larger dimensions of FA with respect to MA is reflected in the resulting average lattice parameter. This high temperature volumetric effect ought to be related to a larger tolerance factor for $FAPbI_3$ ($t_{CsPbI_3} < t_{MAPbI_3} < t_{FAPbI_3}$).[50] The α, β and γ angles of the supercell fluctuate around a mean value of 90° with a standard deviation of 0.6°. The fluctuations observed in the supercell dimensions are accompanied by a relatively fast rotation of the organic cations.[34] The instantaneous local deformations of the inorganic lattice leave elongated cavities to host the organic cations (Figure 1b). From our simulations, the characteristic time for the lattice fluctuations at 450 K amounts to a few ps. Then, averaging the structures over a 20 ps or more leads to cubic structures (Figure 1c), consistent with experimental data.

Further understanding of these *average* cubic structures can be gained when considering

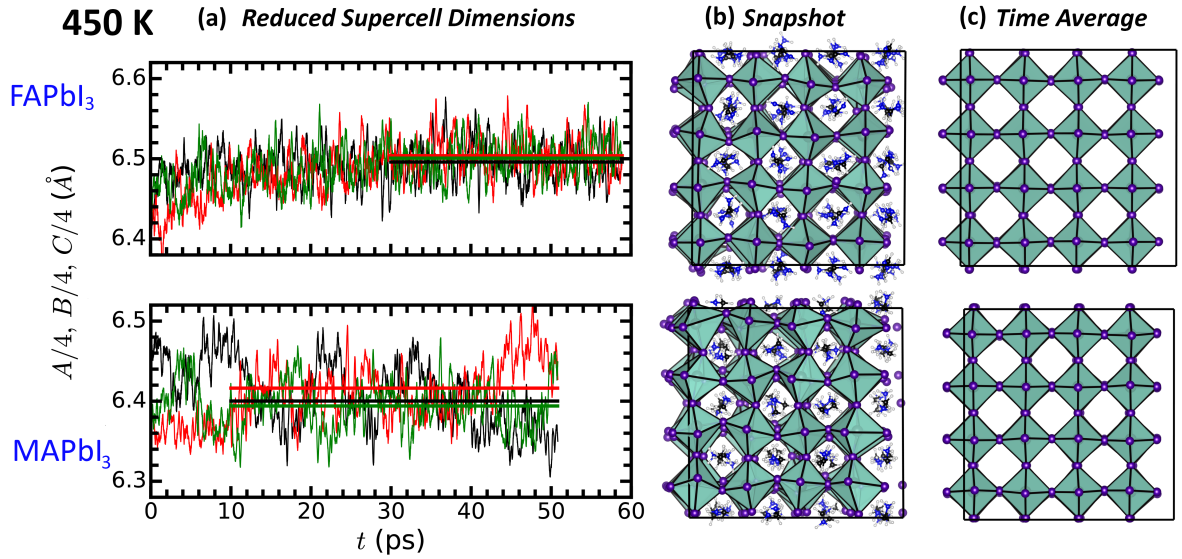

Figure 1: (a) Time evolution of the reduced supercell edges for the hybrid perovskites at 450 K with the horizontal lines representing the mean values over the production fraction of the trajectories. (b) Snapshots displaying the instantaneous deformation of the inorganic lattice and the random orientation of the organic cations. (c) Time average of the inorganic lattice displaying a simple cubic structure.

the anisotropic character of the location of the I atoms in a probabilistic sense. For that, we define the distance δ as the shortest length from the I atom to the straight line connecting the two Pb atoms to which it is bonded (Figure 2a). Then, we can estimate the probability distribution $P(\delta)$ from the MD trajectories. Namely, $P(\delta)d\delta$ is the probability to find an I atom within δ and $\delta + d\delta$ off the line connecting their neighboring Pb atoms. Denoting d_{Pb-I} as the distance between Pb and I atoms, then $\delta = d_{Pb-I} \sin\theta$. The probability is explored around the point $\theta = 0, \forall\phi$ (Figure 2c). First, for $MAPbI_3$ the amplitude of the iodine motion is significantly larger than for $FAPbI_3$, with first moments of the distributions amounting to $\bar{\delta}_{M,450} = 0.679$ Å and $\bar{\delta}_{F,450} = 0.533$ Å, respectively. Second, the probability to have $\delta = 0$ is almost vanishing, which implies that at any time the probability to have a deviation from the perfect cubic unit cell is almost equal to 1. This is an important point and means that the $Pm\bar{3}m$ symmetry reported by the crystallographic experiments must be interpreted as a time average. Within our simulation supercell with 64 units, we are able to

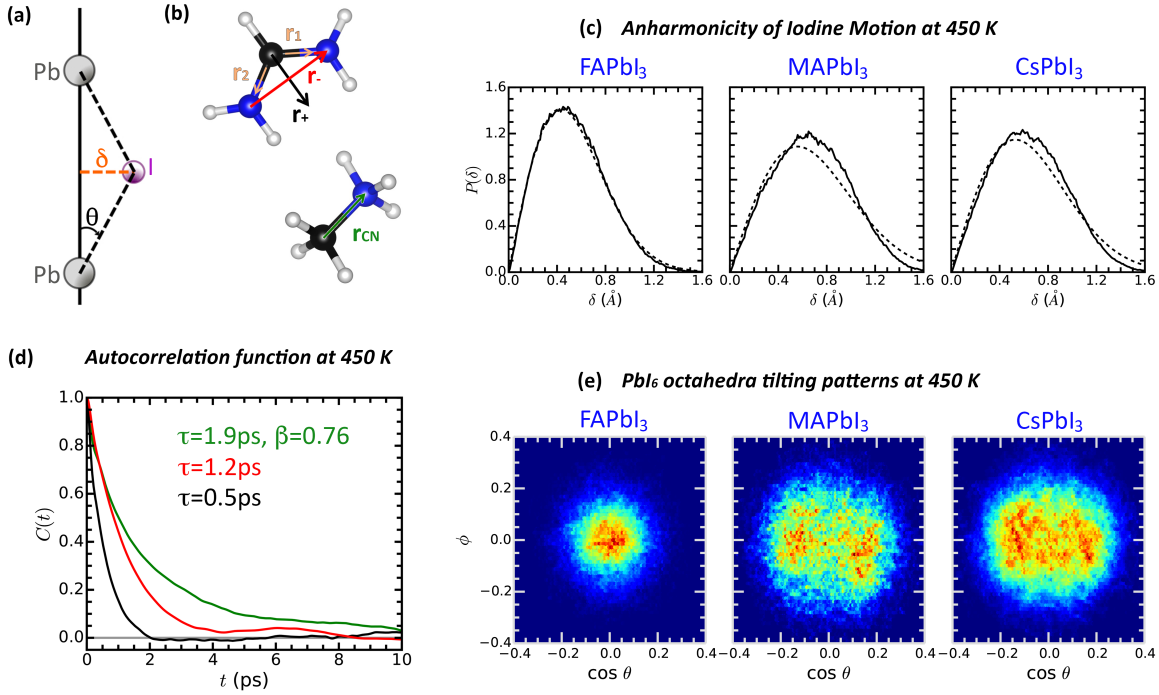

Figure 2: Overall behavior of the hybrid systems at 450 K. (a) Geometrical parameters used to characterize the average an/harmonicity of the systems. (b) Directions used to describe the molecular rotations. (c) Probability distribution for the displacement δ calculated from the MD trajectories (solid lines) and best fits using a harmonic approximation (dashed lines). (d) Self relaxation curves for the different molecular directions, according to the color code defined in panel b. (e) Octahedra tilting patterns.

recover the $Pm\bar{3}m$ symmetry as a time average and we can conclude that for both systems at this high temperature the characteristic lifetime of the transient distorted domains is $t_{lc} \lesssim 20$ ps. The magnitude of the spatial correlations is more difficult to estimate. Visual inspection of many frames along the trajectory reveals that the system follows the same pattern of local deformations over the whole supercell at T=450 K. This pattern smoothly changes with time, but it is difficult to pinpoint a de-correlation between the deformations in local sections of the supercell. Quantitative estimation of λ_{lc} would require a much larger supercell but it is likely that $\lambda_{lc} > 4a$ for both, $MAPbI_3$ and $FAPbI_3$, at $T = 450$ K.

The harmonic or anharmonic character of the atomic fluctuations is important in order to assess the stability of the system using theoretical approximations to the free enthalpy.[19] Namely, it is important to know to what extent it is justified to use the classical quasi-

harmonic approximation for the free energy to make conclusions regarding the stability of a high temperature phase. It is indeed known for the inorganic perovskite $CsSnI_3$, that the quasi-harmonic phonon approximation breaks down, leading in turn to a renormalization of the band gap through self-energy corrections.[51] For the case of hybrid perovskites the problem is in principle more complex since the molecular cation yields additional rotational degrees of freedom. In this scenario, MD simulations offer an opportunity to directly explore the anharmonicity of the atomic fluctuations. Having this in mind we fit the $P(\delta)$ curves using the ideal normal distribution (integrated over the polar angle) that would be the behavior of a purely 2D harmonic oscillator.[52] The best fits are reproduced in Figure 2c for the different systems. The fit is very good only for $FAPbI_3$ at 450 K with the normal curve falling on top of the slightly noisy simulation average. The $MAPbI_3$ at 450 K departs from the normal distribution, with δ stretching to larger values. Interestingly, the $CsPbI_3$ perovskite has a similar anharmonic behavior at T = 450 K than $MAPbI_3$, consistently with experimental results on $CsPbCl_3$.[35] A complementary representation of the displacement of the I atoms from its ideal central position is given by the orientational map for the tilting of the PbI_6 octahedra. These orientational maps represent an approximation to the probability density $p(\theta, \phi)$ for the two dimensional displacement of the I atoms. For small tilting angles, θ and δ are directly related by $\theta d_{Pb-I} = \delta$. Then, the probability distribution for δ can be directly obtained after integration over the azimuthal angle ϕ as $P(\delta) = \int \frac{\delta}{d_{Pb-I}} p(\frac{\delta}{d_{Pb-I}}, \phi) d\phi$. For the sake of simplicity, we show the orientational maps of the simulated structures at 450 K around one particular direction (Figure 2e). $FAPbI_3$ displays a compact spot with a maximum at a centered (not tilted) orientation. $MAPbI_3$ presents a tilting pattern characterized by two off-centered overlapping spots and covering a larger area than for $FAPbI_3$. A similar slightly elongated large spot is observed for the $CsPbI_3$ perovskite. These not centrally symmetric patterns are consistent with the non harmonic distribution observed in δ (Figure 2c).

To evidence the large mobility of the organic cations at 450 K, we plot the relaxation curves of both hybrid systems (Figure 2d). For $MAPbI_3$, the figure reflects the autocorrela-

tion of the NC bonds defined by $\vec{r}_{CN}$. For $FAPbI_3$, the rotational dynamics can be analyzed considering two directions:[28] *i*) the direction along the the sum of the two CN bonds, i.e. $\vec{r}_+$, and *ii*) the direction along the difference between the same two bond vectors, i.e. $\vec{r}_-$ (Figure 2b). The results corresponding to $FAPbI_3$ at 450 K are similar to those already reported[28] and can be fitted with a single exponential function with relaxation time of 1.2 ps and 0.5 ps for $\vec{r}_-$ and $\vec{r}_+$, respectively. The results corresponding to $MAPbI_3$ are obtained following the same simulation methodology to ensure fair and unbiased comparison. Noteworthy, the results presented in Ref.[27] are based on NVT simulations and show some quantitative difference with the ones presented here. The relaxation curve for $\vec{r}_{CN}$ follows a stretched exponential with $\beta = 0.76$ yielding a relaxation time of 1.9 ps. A harmonic coupling between molecular stochastic rotations and phonons is only expected to produce a renormalization of the molecular relaxation time.[27] We thus propose that a stretched exponential behavior results from both, the translation-rotation coupling mechanisms and the onset of anharmonicity for the iodine motion.

3.2 $FAPbI_3$ at 370 K: Weak anharmonicity and lattice deformation coupled to molecular orientation

In ref.[28] we studied $FAPbI_3$ first at 300 K, which after a long trajectory equilibrated to an average $Im\bar{3}$ structure, and then we increased the temperature to reach 450 K. Here we lower the temperature from a well equilibrated 450 K configuration to an intermediate 370 K and extend the trajectory for slightly over 40 ps. The cooling of the system happens smoothly, with the cell dimension slowly decreasing to adjust to new thermal conditions.

At 370 K, $P(\delta)$ of $FAPbI_3$ departs from the ideal normal distribution (Figure 3a) and exhibits similar behavior as MA and Cs based perovskites at 450 K (Figure 2c). The displacement δ of the I atoms from its ideal position along the Pb-Pb connecting lines is slightly larger than for 450 K with a first moment $\bar{\delta}_{F,370} = 0.560$ Å. This is a first indication of the onset of weak anharmonicity for the iodine motion in $FAPbI_3$ at 370 K. In addition, the

three orientational maps for the PbI_6 octahedra (Figure 4a) show a rotation about the x direction, but no rotation about the other two Cartesian directions. This pattern corresponds to $a^0a^0c^+$ tilt in the Glazer notation,[53] after a proper permutation of the axes. A necessary condition for this tilting pattern to occur is that two of the cell dimensions take values slightly smaller than the third one, which is indeed observed. A 30 ps average of the inorganic lattice also evidences a slight deviation from the $Pm\bar{3}m$ symmetry towards a structure having a P4/mbm symmetry (Figure 4b). Taking average structures over shorter times (2 ps) centered at different times along the trajectory reveals that the inorganic framework of $FAPbI_3$ undergoes a slow structural rearrangement which is coupled to the orientation of the molecular cation. Examples are given in Figures 4c and 4d. The first looks mostly cubic, but with some local distortions on the right side of the plot. The second shows the typical alternating pattern resulting from the octahedral tilting, with the orientation of the FA molecules along the longest axes of the cavities. This is a clear indication of the coupling between the local deformations and the molecular orientations.

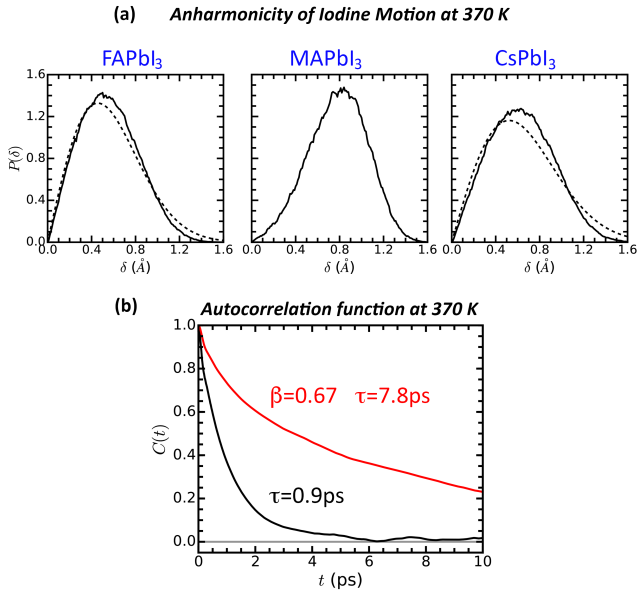

Figure 3: (a) Probability distribution $P(\delta)$ calculated from the MD trajectories (solid lines) and best fits using a harmonic approximation (dashed lines) for the three systems at 370 K. (b) Self relaxation curves for the two different molecular directions (Figure 2b) of the $FAPbI_3$ at 370 K.

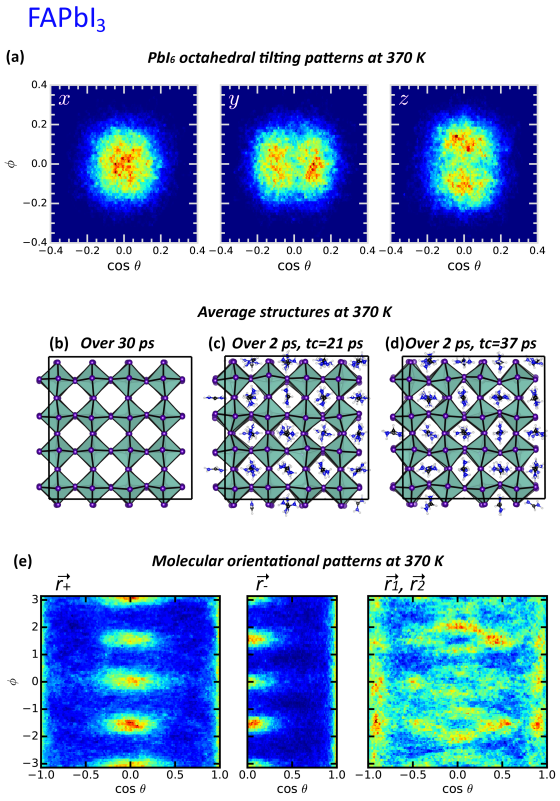

Figure 4: Overall behavior of the $FAPbI_3$ at 370 K. (a) Octahedra tilting patterns for the three Cartesian projections. (b) Long time average conformation of the inorganic lattice. (c) and (d) Short time average conformations at two different times. (e) Orientational maps for the FA molecules as described by its characteristic vectors described in Figure 2b.

The modest distortion of the lattice of $FAPbI_3$ at 370 K, compared to that at 450 K, has an important effect on the molecular kinetics: the rotations around $\vec{r}_+$ are still fast, but the ones about the direction $\vec{r}_-$ undergo a considerable slow down. In fact, at 370 K, the mobility of the FA cations undergo a significant change, with $\vec{r}_-$ following a stretched exponential with $\beta = 0.67$ and a relaxation time of 7.8 ps (Figure 3b). Meanwhile, the behavior of $\vec{r}_+$ can still be fitted using a single exponential with a relaxation time 0.9 ps. To capture the interplay between lattice distortion, molecular orientations and rotational slow down, we further investigate the orientational maps corresponding to the $\vec{r}_+$, $\vec{r}_-$, $\vec{r}_1$ and $\vec{r}_2$ (Figure 4e). The pattern that emerges is one in which the FA molecules are preferably oriented parallel to the supercell axes. Yet, the dynamical character of this phase is reflected by the orientational map of the bond vectors $\vec{r}_1$ and $\vec{r}_2$ that display a large degree of mobility.

Still, when observing the configurations adopted by neighboring FA molecules along the trajectory, it is clear that they organize themselves in alternating orientations matching the largest molecular dimension with the cavity elongation. The overall result and the one for $MAPbI_3$ (vide infra) is consistent with the experimental comparison between $MAPbI_3$ and $FAPbI_3$[24] showing that the first structural instability from the α-phase toward the β-phase occurs at much lower temperature (200 K) in $FAPbI_3$ than $MAPbI_3$. In the simulation, $FAPbI_3$ indeed only exhibits small structural fluctuations and anharmonicity at T=370 K over the simulation time.

3.3 $MAPbI_3$ at 370 K: The importance of the dipolar coupling

The results obtained at 450 K for $MAPbI_3$ are consistent with the experimental evidence of a cubic phase, provided that we consider the average structures. Here we proceed with results obtained after reducing the temperature to 370 K, i.e. 50 K above the experimental transition temperature of $MAPbI_3$ to the tetragonal β phase.[23,24] Repeating our previous analysis (Figure 1), we investigate the time evolution of the reduced supercell dimensions computed at 370 K (Figure 5a). The system size undergoes large fluctuations and after 40 ps, contrary to what was initially expected, two edges of the supercell take a value significantly smaller than the third one. Further analysis triggered us to perform a second, independent simulation that through consistent results. At first glance, one may interpret the transformation of the simulation box as a transition to the tetragonal phase. A closer examination of the system reveals that the structure is reminiscent of the low temperature orthorhombic γ phase, with the MA molecules aligned in an anti-parallel fashion as shown in Figure 5d. Moreover, we observe in Figure 5a that after the transition the lattice constants ratio c/a is slightly larger than 6 %, once again consistent with the orthorhombic phase. The strong displacements of the I atoms with respect to their ideal correlated position is also evidenced. The corresponding probability distribution $P(\delta)$ can be seen in Figure 3a. These findings are in line with the short-range octahedra distortion, similar to that of the

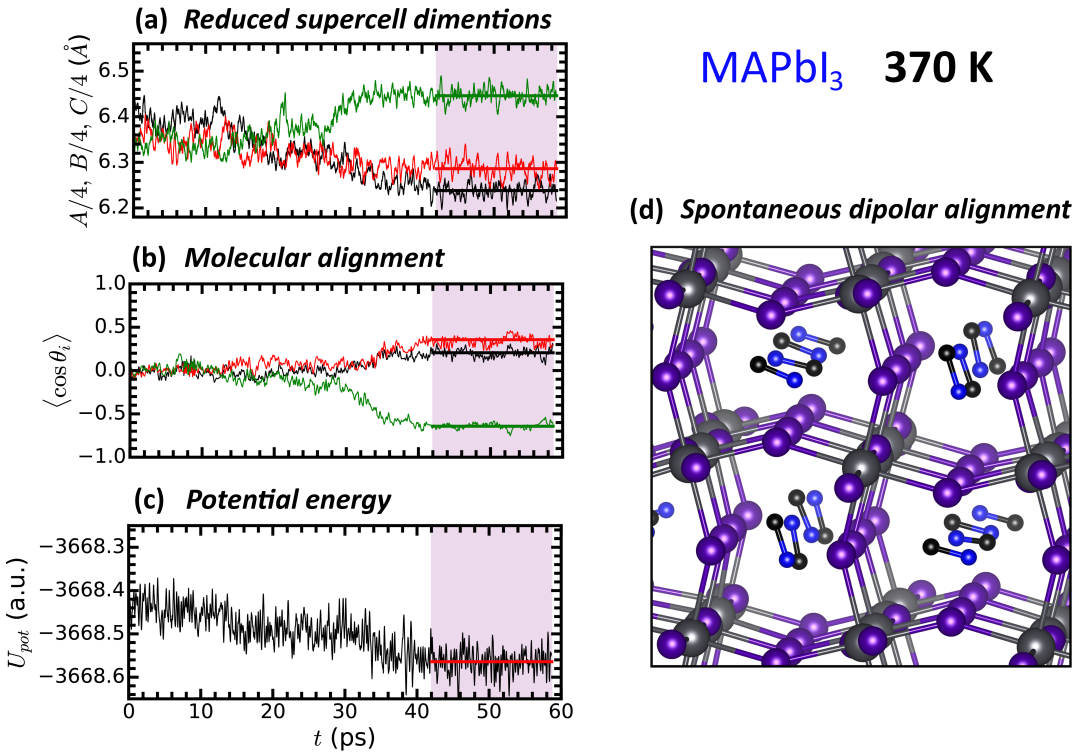

Figure 5: Transformation of $MAPbI_3$ upon cooling. (a) Time evolution of the reduced supercell edges. (b) Average over the supercell of the cosine, $\langle \cos\theta_i \rangle$ for the three Cartesian coordinates, between the direction of neighboring MA molecules (the black, red and green lines represent neighboring cells along the x, y and z directions, respectively). θ_i, with $i = x$, y or z is the angle defined by two neighboring MA molecules. (c) Potential energy of the system as a function of time. d) Conformational average taken in the 42 ps $< t <$ 58 ps interval (shaded area) that shows the lattice deformation and MA alignment.

ordered orthorhombic phase, recently evidenced in both the tetragonal and cubic phases of $MAPbBr_3$.[54]

Now we further explore what is exactly the nature of the phase that the system is transforming to and what is the driving force for the transformation. First of all, we should emphasize that a phase transition in the direction of decreasing entropy is a very rare event in MD simulations, even when using a force-field. Namely, as the new phase requires the spontaneous ordering of all or part of the system, the timescale of this process could be longer than the accessible simulation times. Secondly, when this transition spontaneously occurs, it is quite likely that the new phase is not the one that is thermodynamically stable but an intermediate one. This phenomena also happens in experiments and it is known as

the Ostwald step rule;[55] in an experiment the system will evolve towards the stable phase but in a simulation this second transformation may be unreachable due to time limitation. This might be the case since the phase transition of $MAPbI_3$ from the α (cubic, $Pm\bar{3}m$) to the β (tetragonal, I4/mcm) phase is continuous. In that case, the Landau-Ginzburg theory predicts a divergence of the space (λ_{lc}) and time (t_{lc}) correlation functions related to the order parameter of the phase transition.

To investigate further the changes occurring during the transformation, along with the reduced supercell edge sizes we plot the correlation between neighboring molecular dipoles and potential energy as a function of time (Figures 5b and 5c). The time evolution of the potential energy clearly evidences the transformation towards an average configuration of lower energy after 40 ps. Concomitantly, the rotational dynamic behavior of the MA molecules changes in character. While a relatively high dynamics is observed through the autocorrelation functions of the MA molecules before the transformation, once the new ordering takes place, the dynamics becomes substantially limited. The elongation of the supercell observed for $t > 40$ ps is accompanied by the asymmetrization of the $\langle \cos \theta_x \rangle$ that becomes negative, indicating a majority of antiparallel pairs of MA molecules. This is likely a consequence of coupling between rotations and translations, suggesting a mixed order-disorder/displacive character of the phase transition.

A similar, but not exactly the same, structural ordering was observed recently by Deretzis et al.[36] and Quarti et al.[56]. In both cases, constant volume conditions were used to investigate the cubic and tetragonal phases of $MAPbI_3$ on smaller model systems than in our study. A strong coupling between the molecular orientation and lattice deformation is observed in both cases. However, no antiparallel ordering of the molecular dipoles arises during the simulation time. The reason has to be traced back to the restricted fluctuations in the supercell volume, which are essential to allow for the deformations associated with the full rotation of the MA molecules once the coupling to the lattice deformation has developed.

Besides, the existence of a tricritical point, initially discussed by Kawamura et al.[57] and

recently investigated in details by Whitfield et al.[58], makes it difficult to capture pretransitional fluctuations using ab-initio based MD due to limited computational resources. The latter prevent to explore larger supercell dimensions and hinder extensive sampling of all possible starting configurations.

3.4 Simulation of the tetragonal to cubic transition in $MAPbI_3$

In order to get a better picture and deeper understanding of the response of $MAPbI_3$ to different thermodynamic conditions, within our supercell model, we performed a series of simulations starting from the tetragonal phase. Since the tetragonal phase is typically described using a unit cell that is rotated by 45° around the *c*-axis with respect to the cubic unit cell, the system has to be properly manipulated to match the overall orientation of the simulations for the above-discussed cubic phase. The initial structure was slowly heated to reach 300 K in a series of short runs. Then we performed long runs at 300 K, 320 K, 340 K, 360 K, 370 K, 385 K and 400 K in that sequential order. The behavior of the system for temperatures up to 370 K is quite similar, and only shows a corresponding increase of vibrations around the averaged structure.

The simulations at 385 K and 400 K were both started from the same initial structure obtained from the trajectory at 370 K. For these two temperatures, the system transforms from the original tetragonal structure to a cubic phase. At 385 K the cubic phase is very short lived because the dipolar interaction between neighboring MA molecules starts to play a role and drives the system away from the cubic phase as discussed in the previous section. For the simulation at T = 400 K, once reached, the cubic phase remains stable at least up to 23 ps of the trajectory. The fluctuations emerging in the structure that result in the tetragonal to cubic transformation can be followed along the trajectory of the simulation based on the time evolution of the supercell edge dimensions (Figure 6a). Four zones are distinguished in order to monitor the phase change through the orientational maps of the inorganic octahedra (Figures 6b to 6e). In zone ***i*** the system shows the characteristic tilting of the tetragonal

phase: along the z direction there are no tilting as the Pb-I-Pb bonds are not bent, and the zig-zag bending in the xy plane translate to two spots in each one of the other two tilting projections. In zone ***ii*** the fluctuations in the structure increase and crossings between the main tilting attractors along x and y are observed while the concentrated spot in z gets diffused into a larger area. In zone ***iii*** where the three supercell dimensions start taking similar values, the tilting along the three directions span over similar large areas and the center of the plot (in z) starts to be vacated. The cubic phase is fully reached in zone ***iv*** with the three tilting cases displaying the same qualitative picture of four off centered spots.The later is indicative of iodine displacements of large amplitudes and anharmonicity of optical phonons. Once again, we stress that the $Pm\bar{3}m$ symmetry is reached only on average.

The statistics of the δ parameter (Figure 2a), used to discuss the location of the I atoms, shows an interesting behavior in the tetragonal phase as the system is heated. Figure 7 reports the probabilities $P(\delta)$ for the different simulations performed between 300 and 400 K. At the lowest temperatures, the pattern can be characterized by two peaks, one corresponding to the Pb-I-Pb bonds along the z coordinate, and a second pattern involving the bonds in the plane normal to z. As the temperature increases, the former peak decreases in importance in favor of the later one. At 400 K the system reaches an average cubic phase in zone ***iv***, but one that has a strong anharmonic component. Then, $P(\delta)$ resembles more the previously studied case at 370 K (Figure 3a) than the high temperature result. The reference cubic result at 450 K is included for reference. The evolution of the probability distribution is consistent with the progressive transformation of the dynamics and occupation probability due to an underlying double well potential for the iodine motion.[59] At a critical temperature, a particular phonon mode freezes completely so a static field of displacement of atom positions is induced within the structure.

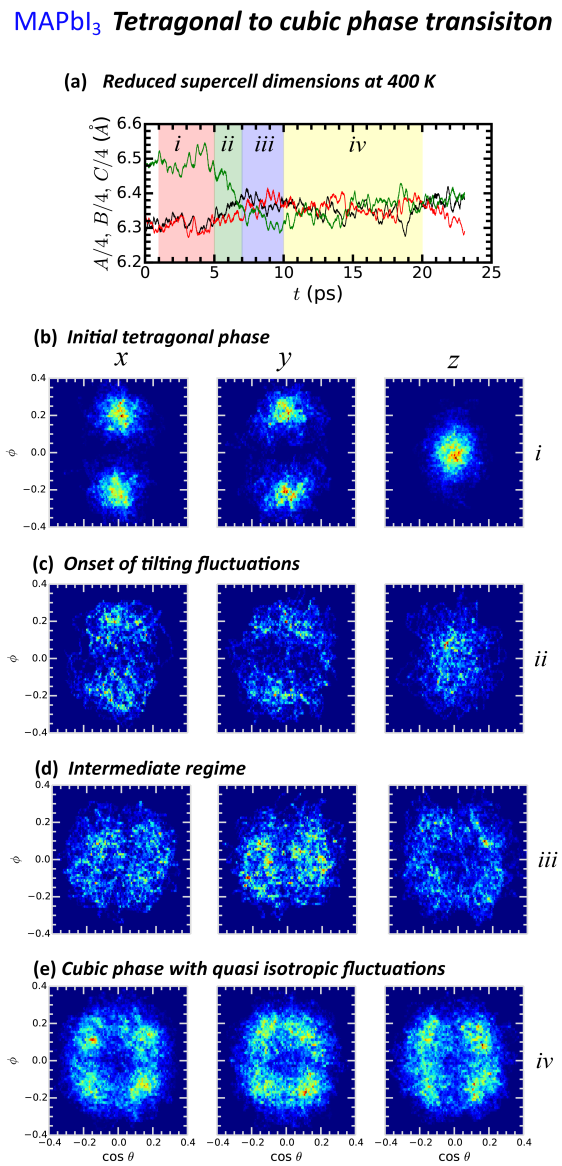

Figure 6: (a) Time evolution of the $MAPbI_3$ phase transformation at T=400 K from the tetragonal to the cubic phase as monitored through the variation of the supercell dimensions. (b) – (e) Variations of the corresponding PbI_6 octahedral tilting patterns represented for the four different time zones highlighted in panel (a)

4 Conclusion

At high temperature, 450 K in our simulations, $CsPbI_3$, $FAPbI_3$ and $MAPbI_3$ reveal all three a cubic structure if considering time averages taken over a lapse larger than a medium lifetime t_{lc}. For our 4×4×4 supercells, $t_{lc} \lesssim 20$ ps at 450 K. We speculate that a spacial average should produce similar results whenever the supercell size is larger than the perovskite characteristic

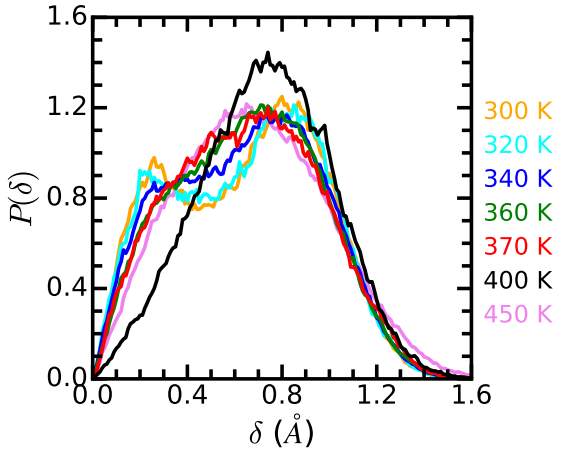

Figure 7: Probability for the I atoms to be located at distance δ from the Pb-Pb connecting line. For $T \leq 400$ K, the curves correspond to trajectories started from the tetragonal phase. For the case at 400 K, $P(\delta)$ was calculated for zone ***iv*** of Figure 6a. For the case at 450 K, the curve is the one corresponding to the cubic phase and included here for reference.

size λ_{lc}. As we do not reach that critical size with our simulation supercell, we can infer that $\lambda_{lc} > 4a$, a being the lattice parameter of the cubic structure.

To capture the anharmonic motion of the iodine atom, the statistical behavior of δ, the distance from the I atom to the line connecting the two Pb atoms to which it is bonded, is very valuable. At high temperature (T=450 K), the only system that undergoes a behavior fully consistent with a harmonic pattern of oscillations is $FAPbI_3$. In fact, $CsPbI_3$ and $MAPbI_3$ display strong supercell fluctuations that are coupled to an anharmonic behavior well reflected by $P(\delta)$. This is consistent with early evidence of anharmonicity from experiments on $CsPbCl_3$.[35] These results should also be related to the tolerance factors of the three structures as $t_{CsPbI_3} < t_{MAPbI_3} < t_{FAPbI_3}$.[50] Indeed, it shows that due to the effective reduced size of the Cs^+ and MA^+ cations, the flexibility of the inorganic framework is favored at high temperature.

At an intermediate temperature (T=370 K), the behavior of $FAPbI_3$ begins to display emergence of weak anharmonicity. Besides, cooling $MAPbI_3$ at the same temperature reveals the importance of the dipolar interactions, which lead the transformation to a different structure. Noteworthy, the phase reached by the system is not the expected tetragonal

phase, but a local structure having antiparallel alignment of MA molecules, which presents some similarities with the low temperature orthorhombic phase. These findings are consistent with the short-range distortions experimentally evidenced in both the tetragonal and cubic phases of $MAPbBr_3$.[54]

Further understanding of the tetragonal to cubic phase transition has been gained thanks to additional simulations where the $MAPbI_3$ structure has been heated starting from the pristine tetragonal phase. At low temperature the probability $P(\delta)$ reveals two different peaks, corresponding respectively to Pb-I-Pb in-plane and out-of-plane bonds. Upon heating both peaks merge into a single one, with progressive built-up of the instabilities leading to an average cubic structure at $T = 400$ K.

Acknowledgements

For computer time, this research used the resources of the Supercomputing Laboratory at the King Abdullah University of Science & Technology (KAUST) in Thuwal, Saudi Arabia and Research Computing group in Texas A&M University at Qatar. Research Computing is funded by the Qatar Foundation for Education, Science and Community Development.

References

(1) Kojima, A.; Teshima, K.; Shirai, Y.; Miyasaka, T. Organometal Halide Perovskites as Visible-Light Sensitizers for Photovoltaic Cells. *J. Am. Chem. Soc.* **2009**, *131*, 6050–6051.

(2) Liu, M.; Johnston, M. B.; Snaith, H. J. Efficient Planar Heterojunction Perovskite Solar Cells by Vapour Deposition. *Nature* **2013**, *501*, 395–398.

(3) Zhou, H.; Chen, Q.; Li, G.; Luo, S.; Song, T.-B.; Duan, H.-S.; Hong, Z.; You, J.; Liu, Y.;

Yang, Y. Interface Engineering of Highly Efficient Perovskite Solar Cells. *Science* **2014**, *345*, 542–546.

(4) Saliba, M.; Matsui, T.; Domanski, K.; Seo, J.-Y.; Ummadisingu, A.; Zakeeruddin, S. M.; Correa-Baena, J.-P.; Tress, W. R.; Abate, A.; Hagfeldt, A. et al. Incorporation of Rubidium Cations into Perovskite Solar Cells Improves Photovoltaic Performance. *Science* **2016**, *345*, 206–209.

(5) Tsai, H.; Nie, W.; Blancon, J.-C.; Stoumpos, C. C.; Asadpour, R.; Harutyunyan, B.; Neukirch, A. J.; Verduzco, R.; Crochet, J. J.; Tretiak, S. et al. High–Efficiency Two–Dimensional Ruddlesden–Popper Perovskite Solar Cells. *Nature* **2016**, *536*, 312–316.

(6) Hattori, T.; Taira, T.; Era, M.; Tsutsui, T.; Saito, S. Highly Efficient Electroluminescence from a Heterostructure Device Combined with Emissive Layered–Perovskite and an Electron–Transporting Organic Compound. *Chem. Phys. Lett.* **1996**, *254*, 103–108.

(7) Chondroudis, K.; Mitzi, D. B. Electroluminescence from an Organic–Inorganic Perovskite Incorporating a Quaterthiophene Dye within Lead Halide Perovskite Layers. *Chem. Mater.* **1999**, *11*, 3028–3030.

(8) Koutselas, I.; Bampoulis, P.; Maratou, E.; Evagelinou, T.; Pagona, G.; Papavassiliou, G. C. Some Unconventional Organic–Inorganic Hybrid Low–Dimensional Semiconductors and Related Light–Emitting Devices. *J. Phys. Chem. C* **2011**, *115*, 8475–8483.

(9) Dohner, E. R.; Jaffe, A.; Bradshaw, L. R.; Karunadasa, H. I. Intrinsic White–Light Emission from Layered Hybrid Perovskites. *J. Am. Chem. Soc.* **2014**, *136*, 13154–13157.

(10) Tan, Z.-K.; Moghaddam, R. S.; Lai, M. L.; Docampo, P.; Higler, R.; Deschler, F.; Price, M.; Sadhanala, A.; Pazos, L. M.; Credgington, D. et al. Bright Light–Emitting Diodes Based on Organometal Halide Perovskite. *Nat. Nanotechnol.* **2014**, *9*, 687–692.

(11) Ling, Y.; Yuan, Z.; Tian, Y.; Wang, X.; Wang, J. C.; Xin, Y.; Hanson, K.; Ma, B.; Gao, H. Bright Light–Emitting Diodes Based on Organometal Halide Perovskite Nanoplatelets. *Adv. Mater.* **2016**, *28*, 305–311.

(12) Kondo, T.; Azuma, T.; Yuasa, T.; Ito, R. Biexciton Lasing in the Layered Perovskite–Type Material $(C_6H_{13}NH_3)_2PbI_4$. *Solid State Commun.* **1998**, *105*, 253–255.

(13) Xing, G.; Mathews, N.; Lim, S. S.; Yantara, N.; Liu, X.; Sabba, D.; Grätzel, M.; Mhaisalkar, S.; Sum, T. C. Low–Temperature Solution–Processed Wavelength–Tunable Perovskites for Lasing. *Nat. Mater.* **2014**, *13*, 476–480.

(14) Li, Y. J.; Lv, Y.; Zou, C.-L.; Zhang, W.; Yao, J.; Zhao, Y. S. Output Coupling of Perovskite Lasers from Embedded Nanoscale Plasmonic Waveguides. *J. Am. Chem. Soc.* **2016**, *138*, 2122–2125.

(15) Edoardo Mosconi, C. Q.; Angelis, F. D. In *Unconventional Thin Film Photovoltaics*; E. Da Como, F. De Angelis, H. Snaith, A. Walker, Eds.; The Royal Society of Chemistry: Cambridge, UK, 2016; pp 234–296.

(16) Whalley, L. D.; Skelton, J. M.; Frost, J. M.; Walsh, A. Phonon Anharmonicity, Lifetimes, and Thermal Transport in $CH_3NH_3PbI_3$ from Many–Body Perturbation Theory. *Phys. Rev. B* **2016**, *94*, 220301.

(17) da Silva, E. L.; Skelton, J. M.; Parker, S. C.; Walsh, A. Phase Stability and Transformations in the Halide Perovskite $CsSnI_3$. *Phys. Rev. B* **2015**, *91*, 144107.

(18) Patrick, C. E.; Jacobsen, K. W.; Thygesen, K. S. Anharmonic stabilization and band gap renormalization in the perovskite $CsSnI_3$. *Phys. Rev. B* **2015**, *92*, 201205.

(19) Marronnier, A.; Lee, H.; Geffroy, B.; Even, J.; Bonnassieux, Y.; Roma, G. Structural Instabilities Related to Highly Anharmonic Phonons in Halide Perovskites. *J. Phys. Chem. Lett.* **2017**, *8*, 2659–2665.

(20) Matsubara, T. Note on the Phase Transition of CuI. *J. Phys. Soc. Japan* **1975**, *38*, 1076–1079.

(21) Matsubara, T. Note on Anharmonic Vibration of Atom in Diamond, Zincblende and Fluorite Structure. *Prog. Theor. Phys.* **1975**, *53*, 1210–1211.

(22) Yang, J.; Wen, X.; Xia, H.; Sheng, R.; Ma, Q.; Kim, J.; Tapping, P.; Harada, T.; Kee, T. W.; Huang, F. et al. Acoustic–Optical Phonon Up–Conversion and Hot–Phonon Bottleneck in Lead–Halide Perovskites. *Nat. Commun.* **2017**, *8*, 14120.

(23) Baikie, T.; Fang, Y.; Kadro, J. M.; Schreyer, M.; Wei, F.; Mhaisalkar, S. G.; Graetzel, M.; White, T. J. Synthesis and Crystal Chemistry of the Hybrid Perovskite $(CH_3NH_3)PbI_3$ for Solid–State Sensitised Solar Cell Applications. *J. Mater. Chem. A* **2013**, *1*, 5628–5641.

(24) Stoumpos, C. C.; Malliakas, C. D.; Kanatzidis, M. G. Semiconducting Tin and Lead Iodide Perovskites with Organic Cations: Phase Transitions, High Mobilities, and Near–Infrared Photoluminescent Properties. *Inorg. Chem.* **2013**, *52*, 9019–9038.

(25) Fabini, D. H.; Hogan, T.; Evans, H. A.; Stoumpos, C. C.; Kanatzidis, M. G.; Seshadri, R. Dielectric and Thermodynamic Signatures of Low–Temperature Glassy Dynamics in the Hybrid Perovskites $CH_3NH_3PbI_3$ and $HC(NH_2)_2PbI_3$. *J. Phys. Chem. Lett.* **2016**, *7*, 376–381.

(26) Carignano, M. A.; Kachmar, A.; Hutter, J. Thermal Effects on $CH_3NH_3PbI_3$ Perovskite from Ab Initio Molecular Dynamics Simulations. *J. Phys. Chem. C* **2015**, *119*, 8991–8997.

(27) Even, J.; Carignano, M.; Katan, C. Molecular Disorder and Translation/Rotation Coupling in the Plastic Crystal Phase of Hybrid Perovskites. *Nanoscale* **2016**, *8*, 6222–6236.

(28) Carignano, M. A.; Saeed, Y.; Aravindh, S. A.; Roqan, I. S.; Even, J.; Katan, C. A Close Examination of the Structure and Dynamics of $HC(NH_2)_2PbI_3$ by MD Simulations and Group Theory. *Phys. Chem. Chem. Phys.* **2016**, *18*, 27109–27118.

(29) Weller, M. T.; Weber, O. J.; Henry, P. F.; Di Pumpo, A. M.; Hansen, T. C. Complete Structure and Cation Orientation in the Perovskite Photovoltaic Methylammonium Lead Iodide Between 100 and 352 K. *Chem. Commun.* **2015**, *51*, 4180–4183.

(30) Sakata, M.; Harada, J.; Cooper, M. J.; Rouse, K. D. A Neutron Diffraction Study of Anharmonic Thermal Vibrations in Cubic $CsPbX_3$. *Acta Cryst.* **1980**, *A36*, 7–15.

(31) Baikie, T.; Barrow, N. S.; Fang, Y.; Keenan, P. J.; Slater, P. R.; Piltz, R. O.; Gutmann, M.; Mhaisalkar, S. G.; White, T. J. A Combined Single Crystal Neutron/X–Ray Diffraction and Solid–State Nuclear Magnetic Resonance Study of the Hybrid Perovskites $CH_3NH_3PbX_3$ (X = I, Br and Cl). *J. Mater. Chem. A* **2015**, *3*, 9298–9307.

(32) Lahnsteiner, J.; Kresse, G.; Kumar, A.; Sarma, D. D.; Franchini, C.; Bokdam, M. Room–Temperature Dynamic Correlation Between Methylammonium Molecules in Lead–Iodine Based Perovskites: An Ab Initio Molecular Dynamics Perspective. *Phys. Rev. B* **2016**, *94*, 214114.

(33) Létoublon, A.; Paofai, S.; Rufflé, B.; Bourges, P.; Hehlen, B.; Michel, T.; Ecolivet, C.; Durand, O.; Cordier, S.; Katan, C. et al. Elastic Constants, Optical Phonons, and Molecular Relaxations in the High Temperature Plastic Phase of the $CH_3NH_3PbBr_3$ Hybrid Perovskite. *J. Phys. Chem. Lett.* **2016**, *7*, 3776–3784.

(34) Roiland, C.; Trippe-Allard, G.; Jemli, K.; Alonso, B.; Ameline, J.-C.; Gautier, R.; Bataille, T.; Le Polles, L.; Deleporte, E.; Even, J. et al. Multinuclear NMR as a Tool for Studying Local Order and Dynamics in $CH_3NH_3PbX_3$ (X = Cl, Br, I) Hybrid Perovskites. *Phys. Chem. Chem. Phys.* **2016**, *18*, 27133–27142.

(35) Fujii, Y.; Hoshino, S.; Yamada, Y.; Shirane, G. Neutron–Scattering Study on Phase Transitions of $CsPbCl_3$. *Phys. Rev. B* **1974**, *9*, 4549–4559.

(36) Deretzis, I.; Di Mauro, B. N.; Alberti, A.; Pellegrino, G.; Smecca, E.; La Magna, A. Spontaneous Bidirectional Ordering of $CH_3NH_3^+$ in Lead Iodide Perovskites at Room Temperature: The Origins of the Tetragonal Phase. *Sci. Rep.* **2016**, *6*, 24443.

(37) Weller, M. T.; Weber, O. J.; Frost, J. M.; Walsh, A. Cubic Perovskite Structure of Black Formamidinium Lead Iodide, α-$[HC(NH_2)_2]PbI_3$, at 298 K. *J. Phys. Chem. Lett.* **2015**, *6*, 3209–3212.

(38) Trots, D. M.; Myagkota, S. V. High–Temperature Structural Evolution of Caesium and Rubidium Triiodoplumbates. *J. Phys. Chem. Solids* **2008**, *69*, 2520–2526.

(39) Lippert, G.; Hutter, J.; Parrinello, M., A Hybrid Gaussian and Plane Wave Density Functional Scheme. *Mol. Phys.* **1997**, *92*, 477–488.

(40) VandeVondele, J.; Krack, M.; Mohamed, F.; Parrinello, M.; Chassaing, T.; Hutter, J. Quickstep: Fast and Accurate Density Functional Calculations Using a Mixed Gaussian and Plane Waves Approach. *Comput. Phys. Commun.* **2005**, *167*, 103–128.

(41) Hutter, J.; Iannuzzi, M.; Schiffmann, F.; VandeVondele, J. CP2K: Atomistic Simulations of Condensed Matter Systems. *Wiley Interdisciplinary Reviews: Computational Molecular Science* **2014**, *4*, 15–25.

(42) Grimme, S. Semiempirical GGA–Type Density Functional Constructed with a Long–Range Dispersion Correction. *J. Comput. Chem.* **2006**, *27*, 1787–1799.

(43) Grimme, S.; Antony, J.; Ehrlich, S.; Krieg, H. A Consistent and Accurate Ab Initio Parametrization of Density Functional Dispersion Correction (DFT–D) for the 94 Elements H-Pu. *J. Chem. Phys.* **2010**, *132*, 154104.

(44) VandeVondele, J.; Hutter, J. Gaussian basis sets for accurate calculations on molecular systems in gas and condensed phases. *J. Chem. Phys.* **2007**, *127*, 114105.

(45) Goedecker, S.; Teter, M.; Hutter, J. Separable Dual–Space Gaussian Pseudopotentials. *Phys. Rev. B* **1996**, *54*, 1703–1710.

(46) Krack, M. Pseudopotentials for H to Kr Optimized for Gradient–Corrected Exchange–Correlation Functionals. *Theor. Chem. Acc.* **2005**, *114*, 145–152.

(47) Martyna, G. J.; Tuckerman, M. E.; Tobias, D. J.; Klein, M. L. Explicit Reversible Integrators for Extended Systems Dynamics. *Mol. Phys.* **1996**, *87*, 1117–1157.

(48) `https://github.com/WMD-group/hybrid-perovskites/blob/master/2015_ch3nh3pbi3_phonons_PBEsol/CH3NH3PbI3_tetragonal.cif`.

(49) McKnight, R. E. A.; Howard, C. J.; Carpenter, M. A. Elastic Anomalies Associated with Transformation Sequences in Perovskites: I. Strontium Zirconate, $SrZrO_3$. *J. Phys.: Condens. Matter* **2009**, *21*, 015901.

(50) Kieslich, G.; Sun, S.; Cheetham, A. K. Solid–State Principles Applied to Organic–Inorganic Perovskites: New Tricks for an Old Dog. *Chem. Sci.* **2014**, *5*, 4712–4715.

(51) Patrick, C. E.; Jacobsen, K. W.; Thygesen, K. S. Anharmonic Stabilization and Band Gap Renormalization in the Perovskite $CsSnI_3$. *Phys. Rev. B* **2015**, *92*, 201205.

(52) Cohen–Tannoudji, C.; Diu, B.; Laloë, F. *Quantum Mechanics* Vol. 1; Wiley: New York, U.S., 1977.

(53) Glazer, A. The Classification of Tilted Octahedra in Perovskites. **1972**, *28*, 3384–3392.

(54) Bernasconi, A.; Malavasi, L. Direct Evidence of Permanent Octahedra Distortion in $MAPbBr_3$ Hybrid Perovskite. *ACS Energy Lett.* **2017**, *2*, 863–868.

(55) Threlfall, T. Structural and Thermodynamic Explanations of Ostwald's Rule. *Org. Process Res. Dev.* **2003**, *7*, 1017–1027.

(56) Quarti, C.; Mosconi, E.; Ball, J. M.; D'Innocenzo, V.; Tao, C.; Pathak, S.; Snaith, H. J.; Petrozza, A.; De Angelis, F. Structural and Optical Properties of Methylammonium Lead Iodide Across the Tetragonal to Cubic Phase Transition: Implications for Perovskite Solar Cells. *Energy Environ Sci.* **2016**, *9*, 155–163.

(57) Kawamura, Y.; Mashiyama, H.; Hasebe, K. Structural Study on Cubic–Tetragonal Transition of $CH_3NH_3PbI_3$. *J. Phys. Soc. Japan* **2002**, *71*, 1694–1697.

(58) Whitfield, P. S.; Herron, N.; Guise, W. E.; Page, K.; Cheng, Y. Q.; Milas, I.; Crawford, M. K. Structures, Phase Transitions and Tricritical Behavior of the Hybrid Perovskite Methyl Ammonium Lead Iodide. *Sci. Rep.* **2016**, *6*, 35685.

(59) Padlewski, S.; Evans, A. K.; Ayling, C.; Heine, V. Crossover Between Displacive and Order/Disorder Behaviour in the Φ^4 Model. *J. Phys.: Condens. Matter* **1992**, *4*, 4895–4908.

Journal of Physical Chemistry C, American Chemical Society, 2017, 121 (38), pp.20729-20738. ⟨10.1021/acs.jpcc.7b08220⟩

TOC Graphic